We are IntechOpen, the world's leading publisher of Open Access books Built by scientists, for scientists

6,900
Open access books available

186,000
International authors and editors

200M
Downloads

Our authors are among the

154
Countries delivered to

TOP 1%
most cited scientists

12.2%
Contributors from top 500 universities

BOOK CITATION INDEX
CLARIVATE ANALYTICS
INDEXED

WEB OF SCIENCE™

Selection of our books indexed in the Book Citation Index
in Web of Science™ Core Collection (BKCI)

Interested in publishing with us?
Contact book.department@intechopen.com

Numbers displayed above are based on latest data collected.
For more information visit www.intechopen.com

The Influence of the Lower Ionospheric Disturbances on the Operating Conditions of Navigation Satellite Systems

Boris Gavrilov, Yuriy Poklad and Iliya Ryakhovskiy

Abstract

The study of the impact of ionospheric disturbances on the conditions of functioning of satellite communication and navigation systems and the development of methods to reduce this effect requires the development of methods for evaluating the parameters of ionospheric disturbances and their spatial and temporal distribution. Studies show that electron concentration disturbances, which can have a significant impact on the functioning of transionospheric radio channels, can occur both in the upper and lower ionosphere. At the same time, the methods of studying the dynamics of ionospheric disturbances in the lower ionosphere are not enough developed, and the interrelation of the lower and upper perturbations of the ionosphere is insufficiently studied. The aim of the work is an experimental study of disturbances of the upper and lower ionosphere in order to clarify the mechanisms of their relationship and study the spatiotemporal distribution of mid-latitude disturbances. The results obtained show that the contribution of the electron density disturbances in the D region to the total electron content of the ionosphere can be significant and considerably depends on the type of heliogeophysical processes.

Keywords: upper and lower ionosphere, traveling ionospheric disturbances, TEC, VLF signals, magnetic storms, solar X-ray flares

1. Introduction

The ionosphere is a region in the near-Earth space, where a number of technical systems vital for the life and safety of mankind (telecommunication, navigation, aircraft, surveillance systems, etc.) work continuously. These systems based on radio signals are sensitive to the varying electron density in the ionosphere. Its strong perturbations may cause failures and malfunction in these systems. So the investigation of the state and dynamics of the ionosphere and a prediction of irregularities and disturbances appearing are key questions.

Ionospheric disturbances are closely related to geomagnetic storms, solar flares, and other natural and anthropogenic processes [1–6]. The effect that the lower and upper ionospheres have on the propagation of a radio signal depends on their frequency. The F region is critical for the propagation of high-frequency (HF) waves. State and dynamics of the D and E regions define the conditions of

propagation of low-frequency (LF) and very low-frequency (VLF) waves. Due to these reasons, HF and LF-VLF waves can be used to study F and D–E regions, respectively.

The impact of the processes of interaction in the lithosphere, atmosphere, ionosphere, and magnetosphere system on the upper and lower ionosphere and radio wave propagation was studied for decades [7–10]. Total electron content (TEC) values determined from data of dual-frequency measurements of global navigation satellite system (GNSS) signals are widely used to study the state and dynamics of the ionosphere [1, 3, 5, 6]. TEC is an integral of electron density in a tube with a cross section of 1 m^2 along the path of radio signal propagation from the navigation satellite to the receiver. It is assumed that TEC value mainly characterizes the state of the F region where (at least in quiet heliogeophysical conditions) the maximum electron density is observed.

Obtaining direct data on the state and dynamics of the lower ionosphere is a more complex experimental task, since at these altitudes the ionosondes, radars, and spacecraft practically do not work. The state of the lower ionosphere is often monitored by analyzing the characteristics of VLF (3–30 kHz) radio signals that propagate in the waveguide formed by the Earth's surface and the D region of the ionosphere. Variations in the amplitude and phase of VLF signals are mainly associated with changes in the state of the upper wall of the waveguide [11–13].

Despite the fact that both methods of ionosphere studying are quite effective, they are used separately as a rule, which does not allow investigating the relationship between the disturbances of the upper and lower ionosphere.

The focus of this article is an experimental study of the relationship between the perturbations of the upper and lower ionosphere.

The experiments were carried out during a strong geomagnetic storm and strong solar X-ray flares. Total electron content (TEC) data obtained from measurements of global navigation satellite system (GNSS) signals were used to study the F region. Information about the disturbances of the lower ionosphere is obtained by analyzing the amplitude and phase variations of VLF signals. Coordinated analysis of TEC and VLF signals is a powerful tool for studying interrelated processes in the D and F regions of the ionosphere. The results obtained strongly indicate their interconnected perturbations.

2. Experimental setup

Disturbances of the electron density and radio wave propagation in the D, E, and F regions of the ionosphere were investigated in the latitude range from 40° to 70° N and in the longitude range from 0° to 40° E. The "Mikhnevo" geophysical observatory (MIK, 54.9617° N, 37.7626° E) of the Institute of Geosphere Dynamics of the Russian Academy of Sciences (http://idg.chph.ras.ru/ru/watch/mikhnevo) continuously monitors the amplitudes and phases of signals in the frequency band from 9 to 30 kHz received from VLF stations located in Europe, Asia, and North America [14].

For the investigation of the upper ionosphere, we use the data of GPS receivers in Mikhnevo observatory and the worldwide GPS vertical TEC data included in the Madrigal database at MIT Haystack Observatory (http://www.openmadrigal.org/).

The Madrigal data contain TEC values with a time step of 5 min. These data were averaged over a 15-min interval and distributed over the 180° × 360° grid with a step of 1°.

The deviation of TEC from the median value is calculated by the formula

$$\Delta TEC(lat, long, t) = TEC(lat, long, t) - M, \qquad (1)$$

where lat and long are latitude and longitude, t is UT, and M is the median value of TEC for the previous 27 days for the point with coordinates lat and long.

The equipment used to make the VLF signal measurements is the Metronix Analog/Digital Signal Conditioning Unit ADU-07 data logger connected to Metronix MFS-07 magnetic field sensor. MFS-07 is a high-frequency induction coil magnetometer, and two are mounted along the geographic north-south (X) and east-west (Y) axes. The magnetic field sensors cover a wide frequency range from 1 mHz up to 50 kHz and a dynamic range >130 dB and have excellent low noise characteristics (5×10^{-7} nT/$\sqrt{Hz}$ at 1000 Hz). ADU-07 unit and MFS-07 induction coils have a very stable transfer function over temperature and time. A GPS clock provides the timing signals.

Radio signals with a frequency below 30 kHz propagate in the Earth-ionosphere waveguide at distances of thousands and tens of thousands of kilometers with low attenuation. The relationship of the amplitude and phase of the VLF signal on the state of the D layer makes it possible to detect disturbances of the lower ionosphere in the path of the radio signal propagation. The transmitting stations were chosen so that the radio paths were under different azimuths over the territory of Europe. In our experiments the data of synchronous measurements and the signals from four transmitters were used: JXN (Gildeskål, Norway, 66.98° N, 13.87° E), GQD (Anthorn, UK, 54.91° N, 2.27° W), GBZ (Skelton, UK, 54.73° N, 2.88° W), and NAA (Cutler, USA, 44.65° N, 67.28° W).

When analyzing the parameters of the VLF signal, it should be taken into account that their variations are associated with changes in the parameters of the upper wall of the waveguide along the entire path of signal propagation. In order to localize disturbances in the lower ionosphere, data on the signal propagation along the path were additionally used, crossing the paths JXN-MIK, GQD-MIK, and NAA-MIK. We chose the data of Kiel Longwave Monitor (http://www.lf-radio.de/) where signals were received from Norwegian transmitter JXN (66.96° N, 13.90° E).

Radio signals received at the MIK and Kiel (54.4° N, 10.1° E) observatories were compared with data on variations in TEC of the ionosphere according to the Scripps Orbit and Permanent Array Center (SOPAC) http://sopacold.ucsd.edu/dataBrowser.shtml and Madrigal (http://www.openmadrigal.org) databases. Since we were
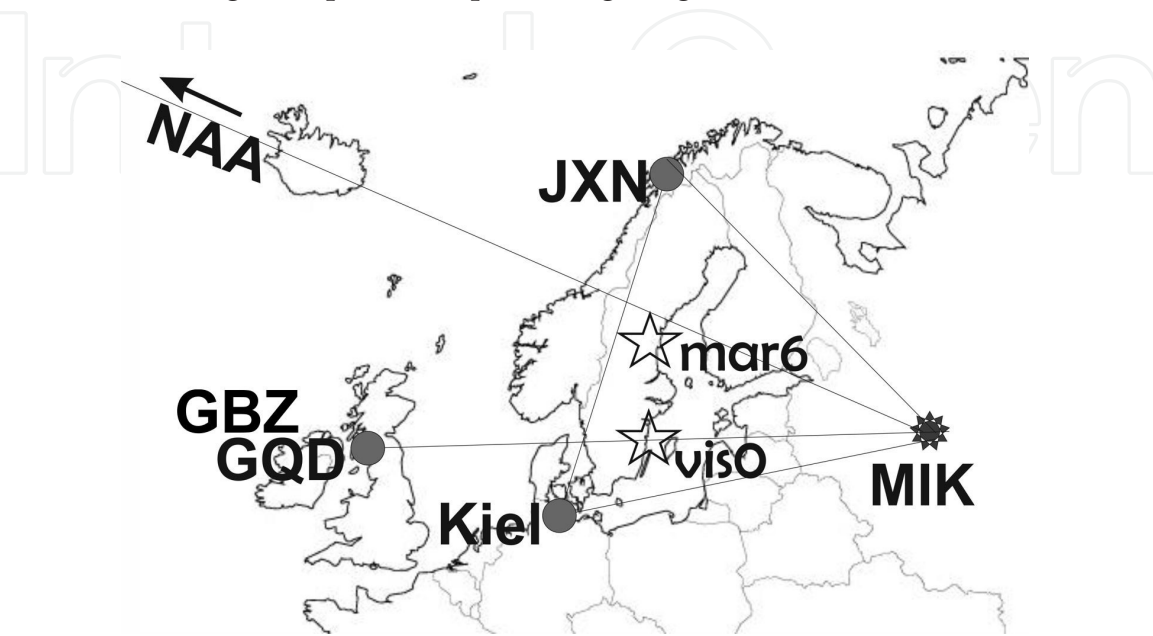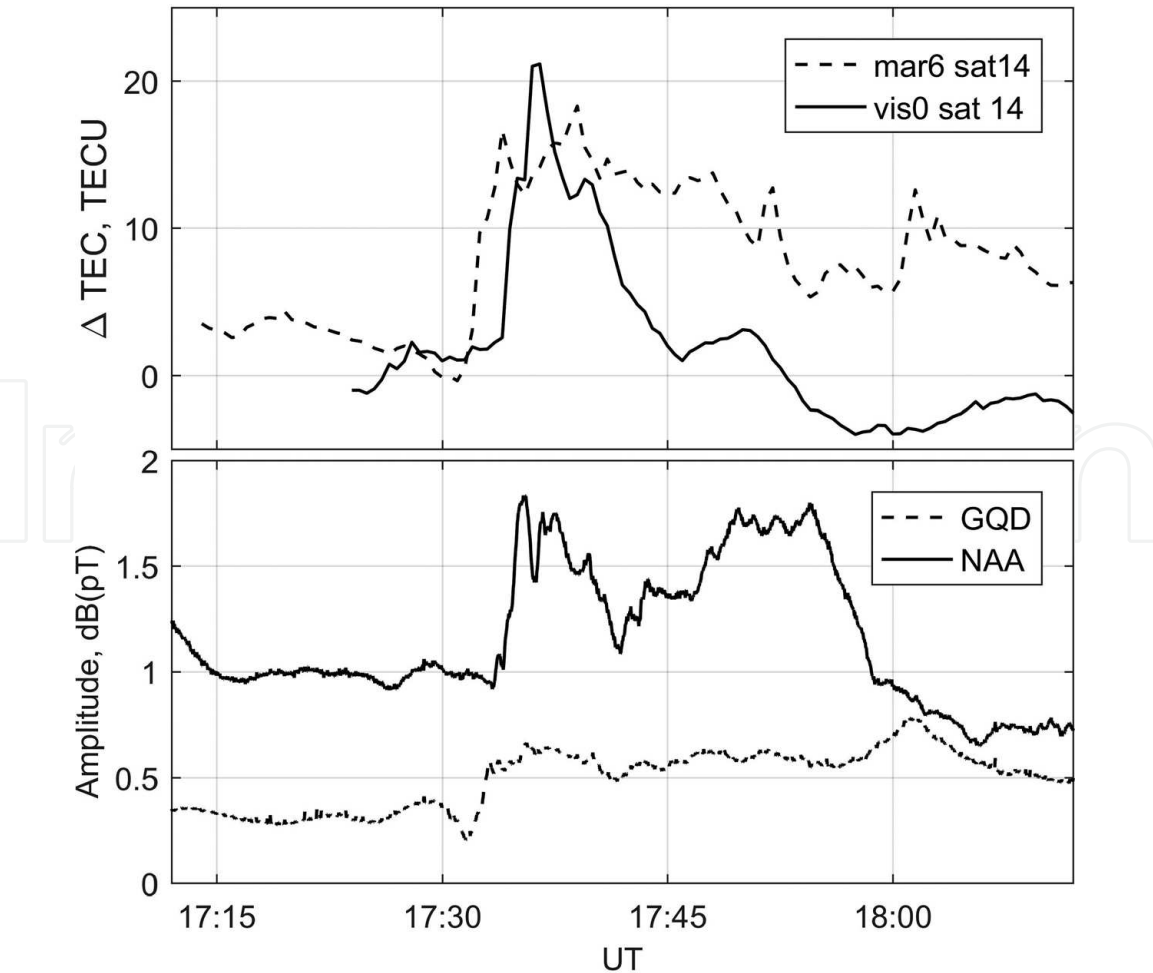

Figure 1.
The location of VLF transmitters (gray circles), GPS receivers (asterisks), and MIK observatory.

interested in the interrelated perturbations of the upper and lower ionospheres, GPS stations located near the used VLF signal traces were chosen. The location of the transmitters and measuring stations is shown in **Figure 1**.

The possibility of detection of interconnected disturbances in the upper and lower ionosphere by GPS and VLF receivers is shown by the example of the study of the ionospheric effects of the magnetic storm on 17 March 2015 and the solar X-ray flash on 6 September 2017. These events were chosen because they caused significant changes in the ionosphere, but the mechanisms of generation and evolution of ionospheric inhomogeneities during magnetic storms and solar X-ray flares are very different, which should be manifested in the pattern of the reaction of the D and F layers of the ionosphere to these phenomena.

3. St. Patrick's Day geomagnetic storm

The storm began on 15 March 2015 as a series of mid-level solar flares culminating in a class C9 flare at 02:13 UT. At 04:05 UT on 17 March 2015, the Advanced Composition Explorer (ACE) satellite recorded a sharp increase in the solar wind speed up to 500 km/s. The lowest value of the disturbance storm time index Dst exceeded 200 nT, the auroral activity index AE exceeded 2200, and the planetary index of the geomagnetic activity Kp reached a value of 8. Such values of these indices make it possible to define the event on 17 March 2015 as an extreme magnetic storm, which caused a storm in the ionosphere.
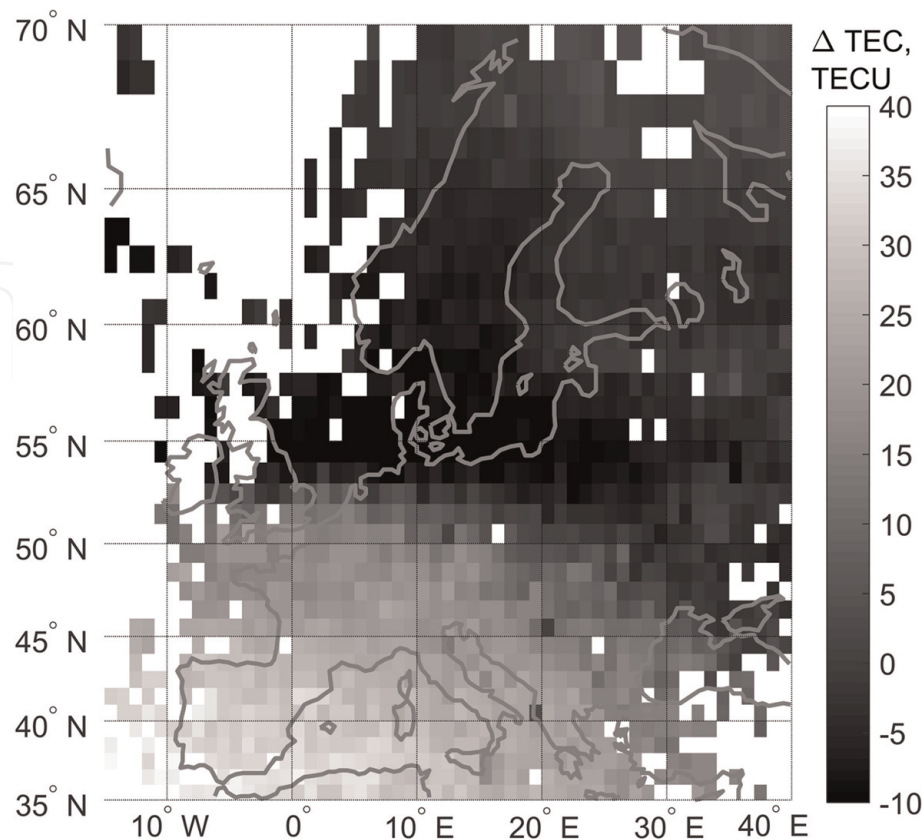

Figure 2.
Variations of TEC according to observatories mar6 and vis0 (top panel), VLF signal amplitude on NAA and GQD-MIK paths (bottom panel) on 17 March 2015.

The strongest geomagnetic storm in the current solar cycle has been studied in sufficient detail. Ground-based and space-born measurements demonstrate the response of the ionosphere to the geomagnetic storm. Astafyeva et al. and Borries et al. [15, 16] presented the results of investigation of the effects of the St. Patrick's Day ionospheric storm from the data of ground-based the GPS receivers,
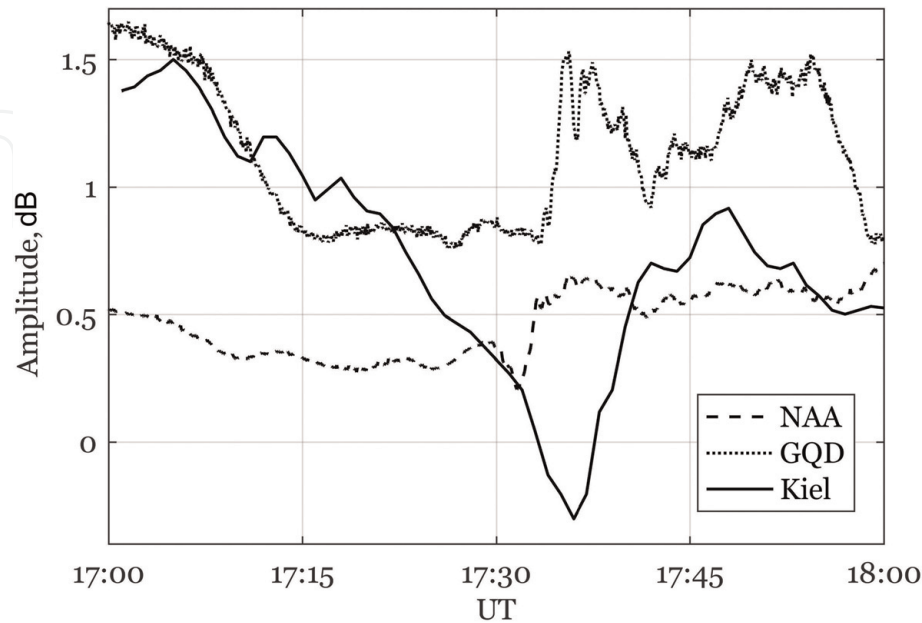
Figure 3.
Variations of VLF signal amplitude on GQD, NAA-MIK paths and on JXN-Kiel path (http://www.lf-radio. de/) from 17 to 18 UT on 17 March 2015.

Figure 4.
The ΔTEC value determined by Eq. (1) for 17.5 UT on 17 March 2015.

ionosondes, and satellite missions. They reveal both a positive effect (TEC increase) at low- and mid-latitudes and positive and negative phases throughout all the latitudes. So, the results of these studies are mostly related to disturbances in the F region of the ionosphere. The effect of the magnetic storms in the lower ionosphere is less known due to the limited possibilities of ionosondes and incoherent scattering radars for the investigation of this region. Our data should allow to compare the results of the study of the F layer of the ionosphere with the effects observed in the lower ionosphere.

The upper panel of **Figure 2** shows the ionospheric variations of TEC calculated from data of GPS receivers located at stations vis0 and mar6. The lower panel shows the VLF signal amplitude variations on the NAA-MIK and GQD-MIK paths. TEC disturbances and VLF signal variations correspond to the main phase of the magnetic storm.

The **Figure 3** shows the change in the VLF signal amplitude on the JXN-Kiel path together with signals on the GQD-MIK and NAA-MIK paths. The maximum amplitude of all signals also corresponds to the main phase of the storm.

Figure 4 shows the distribution of TEC deviation from the previous 27 days over Europe at 17:30 UT according to data of the Madrigal network. The Madrigal data contain TEC values with a time step of 5 min. These data were averaged over a 15-min interval and distributed over the geographic grid with a step of 1°.

It can be seen that the strongest ionospheric perturbations are localized at this time in the region of our measurements around the Kiel and along the GQD-Mikhnevo path.

4. Ionospheric effects of the solar X-ray flares in September 2017

The solar X-ray flares were chosen as another high-energy event, different from the magnetic storm by the mechanisms of influence on the ionosphere. The main perturbation agent of the ionosphere is X-ray and ultraviolet radiation.

Monitoring of VLF signals is conducted in the Mikhnevo since 2014. The most powerful solar X-ray flares for this period occurred in early September 2017. Two solar X-ray flares X2.2 at 09 UT and X9.3 at 12 UT were observed on 6 September 2017. 10 September 2017 was observed X8.3 flare. But at this time, our receivers in Mikhnevo and part of VLF paths were in the region of evening terminator. So its flare was not used in our analysis.

To analyze flare effects in the upper and lower ionosphere, we used the same GPS stations and the same VLF signal paths that were used at observing the effects of the magnetic storm on 17 March 2015. Note that all measuring points and radio paths were located in the territory illuminated by the flashes.

Graphs of vertical TEC variations at flare 6 September 2017 at 12 UT according to GPS receiver located at mar6 and vis0 stations are shown in **Figure 5a**. Variations in the amplitude and phase of the radio signal received in the Mikhnevo from two VLF radio transmitters (GQD and NAA) are shown in **Figure 5b** and **c**. The maximum response to the flare was observed at 12 UT as a simultaneous jump in the ΔTEC and in phase and amplitude of VLF signals.

Comparing **Figures 2** and **5**, we can conclude that the growth of TEC during the X-ray flash was about 10 times less and the increase in the amplitude of the VLF signal was about 5 times greater than during the magnetic storm. To evaluate the effect of the X-ray flash on the additional ionization of the D layer, it is necessary to use theoretical models that allow to relate the parameters of the VLF signals to the change in the parameters of the lower ionosphere.
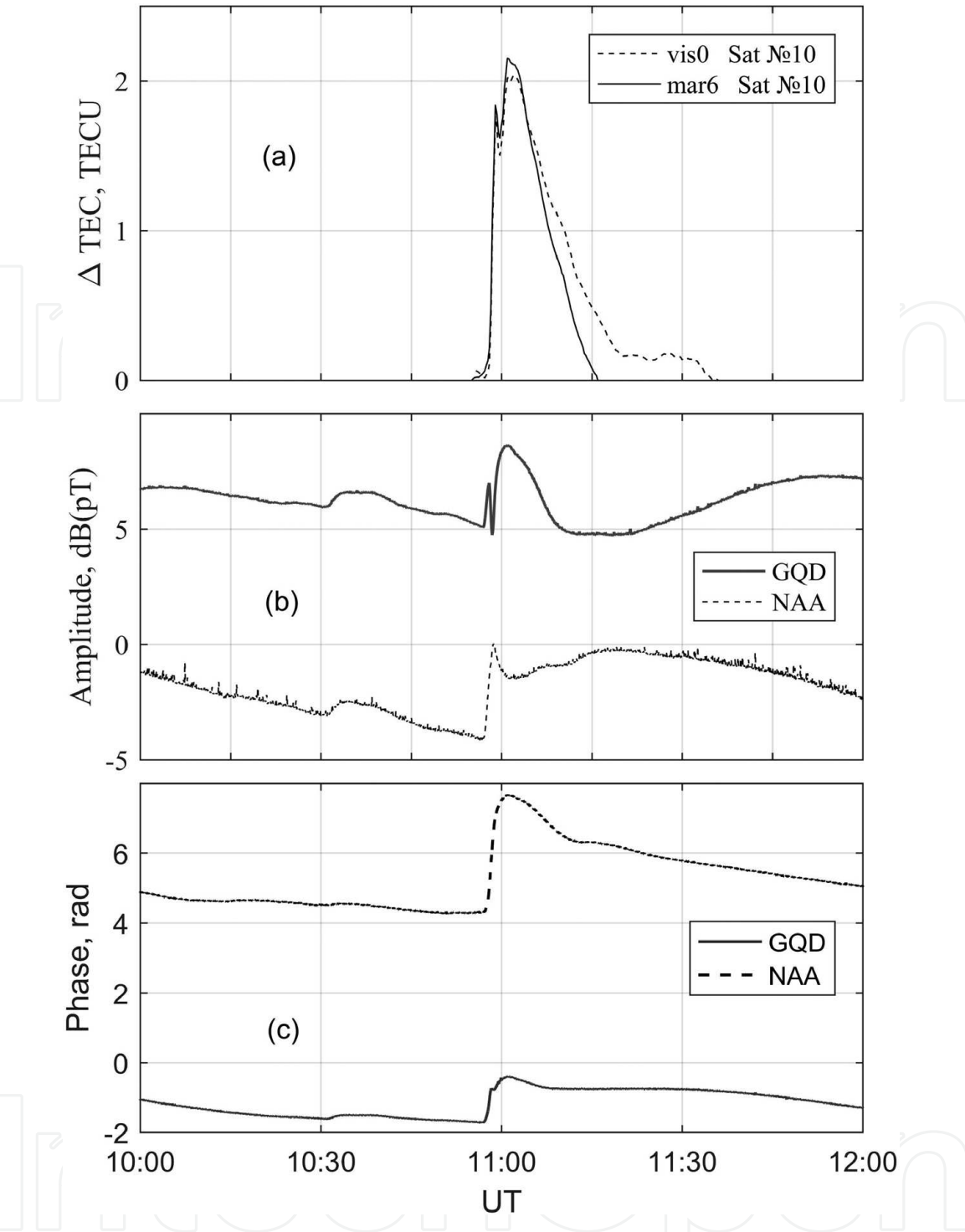
Figure 5.
(a) Variations of TEC according to GPS receiver mar6, (b) amplitude, and (c) phase of VLF signals on the paths JXN-MIK, GQD-MIK, and NAA-MIK on 6 September 2017.

One of the most common ways to describe the D region is the Ferguson-White model [17, 18]. According to this model, the altitude profile of the electron concentration in the lower ionosphere is described by the equation:

$$Ne(z) = 1.49 \cdot 10^7 \cdot \exp\left((\beta - 0.15)(z - h')\right) \cdot \exp\left(-0.15h'\right) \quad [cm^{-3}] \quad (2)$$

where h' is the referenced altitude of the ionosphere, β is the slope factor or sharpness of the electron concentration profile, and h is the current height.

The approach proposed in [19] can be used to estimate variations of these ionospheric parameters during solar flares. In this work, the effects of solar energetic phenomena on the lower ionosphere using parameters of subionospherically

propagating VLF signals were studied. This is done in two steps. At the first stage, initial values of h' and β are selected for this VLF signal propagation path from empirical models [20–22] that take into account the impact on the value of h' and β zenith angle of the sun, latitude, day of the year, and solar activity in the form of the Wolf number. In the second stage, the standard for estimation of the VLF signals propagation Long Wavelength Propagation Capability (LWPC) code is used to estimate the amplitude change in the exponential ionosphere. As a result, the values of h' and β as a function of the X-ray flux were obtained.

The disadvantage of this approach is that the actual state of the ionosphere before a flash may differ from the model due to disturbances from such effects as magnetic storms and an increased X-ray flux.
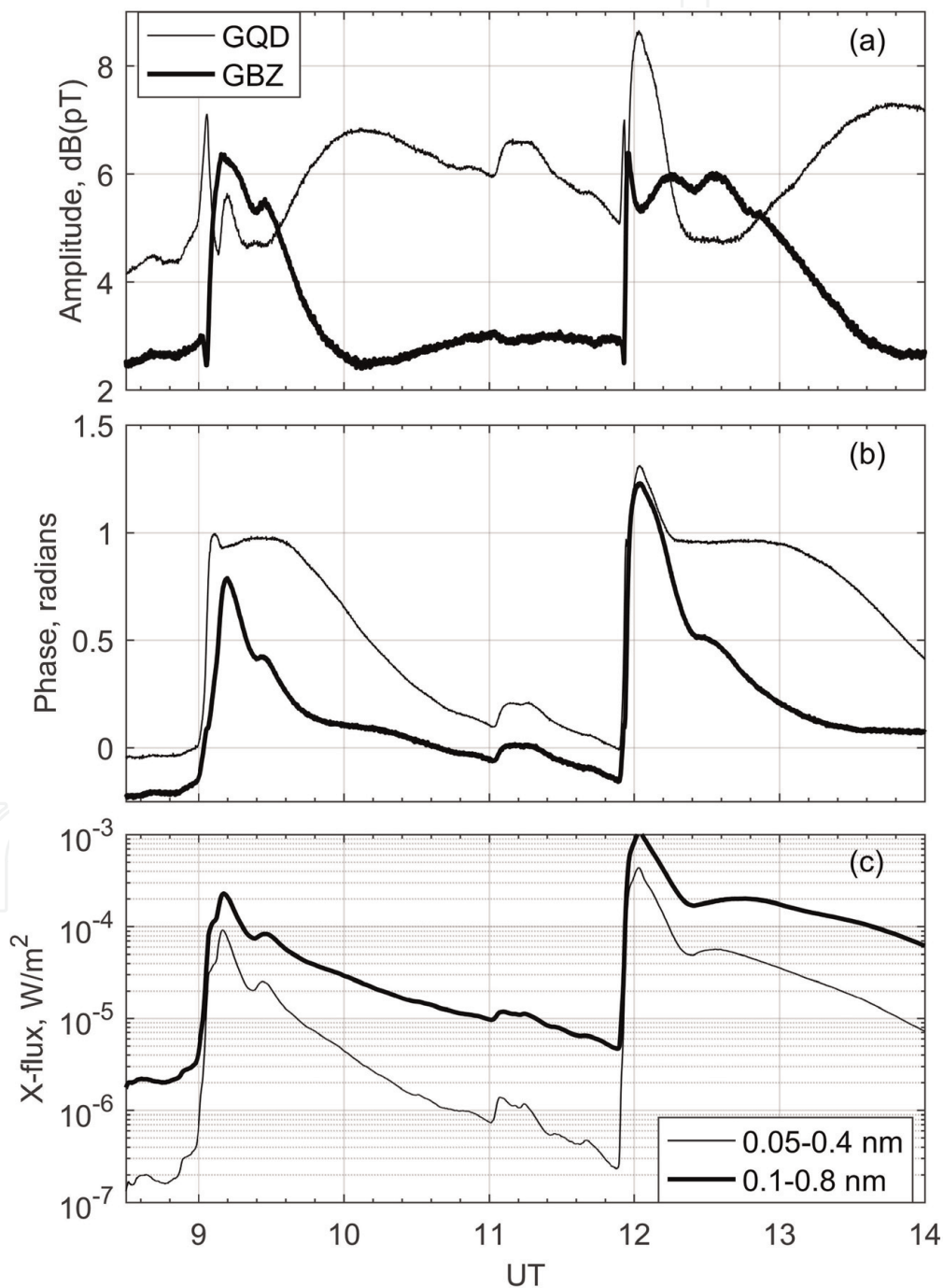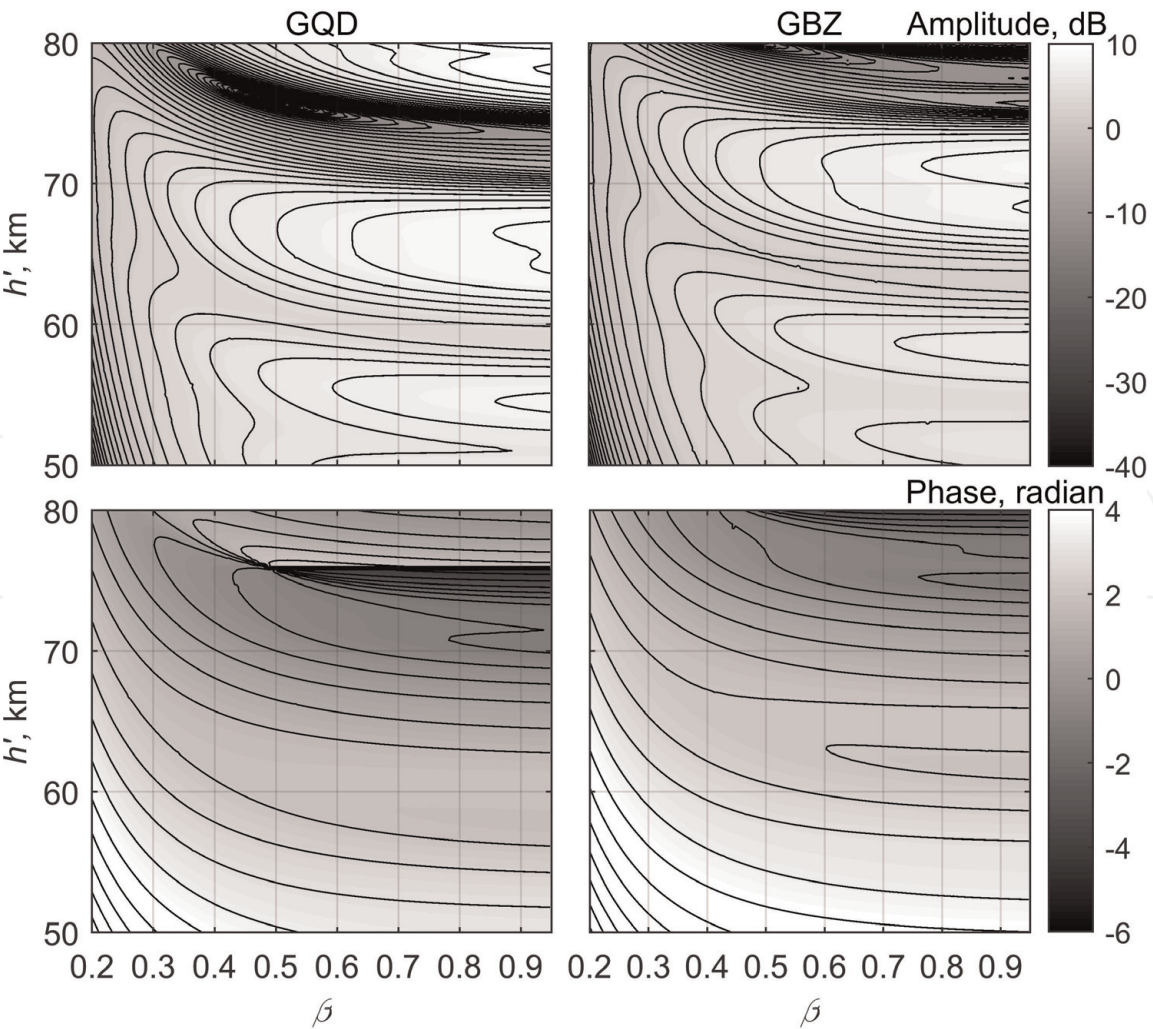

Figure 6.
Variations of the amplitude A * (a) and phase P* * (b) of the signals from GQD and GBZ transmitters and X-ray flux (c) from GOES 15 satellite data (https://www.polarlicht-vorhersage.de/goes/2017-09-06_110000_2017-09-06_130000.png) on 6 September 2017.*

In this paper, a different approach is used to evaluate changes in the lower ionosphere caused by X-ray flashes. The key difference between our method and [19] is the approach to determining the parameters of the ionosphere. We obtain initial conditions by processing experimental data on the amplitude and phase of VLF signals under the action of X-rays. We have developed a method for restoring the altitude profile of electron concentration in the D region of the ionosphere by using the amplitude and phase characteristics of signals from VLF transmitters on a two-frequency path. To implement this technique, the signals of two VLF transmitters located at a distance of 32 km from each other were used. GQD and GBZ transmitters operate at frequencies of 22.1 and 19.58 kHz, respectively. Taking into account the length of the path of about 2600 km, we can assume that the signals from these two stations are distributed along one two-frequency path.

The key difference between our method and [19] is the approach to determine the parameters of the undisturbed ionosphere. Statistical data do not take into account the impact on the ionosphere of factors not described by empirical models. We obtain initial conditions by processing experimental data on the amplitude and phase of VLF signals under the action of X-rays.

Let us consider in detail this technique on the example of ionosphere parameter recovery during X-ray flash of class X9.3 on 6 September 2017.

Figure 7 shows the experimental data on the variations of the amplitude and phase of the signals from GQD and GBZ stations. The bottom panel shows the X

Figure 7.
The calculated values of the amplitude (top panel) and phase (bottom panel) signals of the stations of GQD и GBZ.

flux in two spectral bands according to the Geostationary Operational Environmental Satellite (GOES) data.

Denote the X9.3 flash start time as t_0 = 11:52:20 UT and the time of maximum radiation as $t_{\max}$ = 12:02:14 UT. Let variations of the amplitude and phase $dA_i(t)$ and $dP_i(t)$ be determined as

$$dA_i(t) = A_i^*(t) - A_i^*(t_0)$$
$$dP_i(t) = P_i^*(t) - P_i^*(t_0) \tag{3}$$

where A_i^* and P_i^* are the measured amplitudes and phases of the signals of the GQD (i = 1) and GBZ (i = 2) transmitters shown in **Figure 6**.

On the other hand, the amplitude and phase of the signals of the GQD and GBZ transmitters depend on the parameters of the ionosphere h' and β on the signal propagation path. Suppose that for the whole GQD-/GBZ-Mikhnevo path, the parameters h' and β are the same. Then, the amplitude and phase values of the signals from the transmitters for all possible pairs of h' and β values were calculated using LWPC code. This code allows to calculate amplitude and phase of the VLF signal for the given path and the values of h' and β parameters. The calculations were carried out in the range of 50–90 km with 0.035 km increments for h' and 0.2–0.95 km^{-1} with 0.001 km^{-1} increments for β. The ranges of values of h' and β were selected according to [20–22]. Thus, four matrices with the size of 1143 × 751 elements with values of amplitudes and phases of VLF signals versus h' and β parameters were obtained. Let us denote the calculated values of the amplitude and phase as $A_i(h', \beta)$ and $P_i(h', \beta)$, where i = 1 for GQD and i = 2 for GBZ transmitters. The graphical representation of these data is shown in **Figure 7**.

Let us denote the parameters of the ionosphere at a time t_0 as h_0' and β_0 and at a time $t_{\max}$ as h_{max}' and $\beta_{\max}$. In the matrices $A_i(h', \beta)$ и $P_i(h', \beta)$, we can find all pairs of points (h_0', β_0) and $(h'_{\max}, \beta_{\max})$ for which the difference between the values of amplitudes and phases for t_0 and $t_{\max}$ coincides with that measured with given precision:

$$\left| A_i\left(h'_{\max}, \beta_{\max}\right) - A_i(h_0', \beta_0) - dA_i(t_{\max}) \right| < \delta A$$
$$\left| P_i\left(h'_{\max}, \beta_{\max}\right) - P_i(h_0', \beta_0) - dP_i(t_{\max}) \right| < \delta P \tag{4}$$

where δA = 0.12 dB and δP = 0.06 rad are the accuracy of estimation of the parameters of the ionosphere.

Based on the data [20–22], we assume that the parameters of the ionosphere at t_0 lie in the range of 68 < h_0' < 77 km and 0.22 < β_0 < 0.35 and the parameters of the ionosphere at the $t_{\max}$ lie in the range of 54 < $h_{\max}'$ < 68 and 0.31 < $\beta_{\max}$ < 0.95.

The regions of existence of pairs of points (h_0', β_0) and $(h_{\max}', \beta_{\max})$ that satisfy condition Eq. (4) are shown in **Figure 8** by extended gray areas. They show the entire possible range of ionospheric parameters before the flash Eq. (1) and at maximum X-ray radiation Eq. (2).

The range of the obtained parameter values is quite wide. Let us try to narrow down the ranges of values of h_0' and β_0. To do this, according to Eq. (3), we calculate the variations of the amplitude and phase of the signals for a time step of 15 seconds. So, for time from t_0 to $t_{\max}$, we obtained 39 intermediate values of the variations of amplitudes and phases of the signals from the transmitters. Among the family of points (h_0', β_0), we find those for which there are such points (h_t', β_t) and for which the variation of amplitude and phase corresponds to that measured for all registered intermediate values:

$$\left| A_i\left(h'_t, \beta_t\right) - A_i(h'_0, \beta_0) - dA_i(t)\right| < \delta A \\ \left| P_i\left(h'_t, \beta_t\right) - P_i(h'_0, \beta_0) - dP_i(t)\right| < \delta P \qquad (5)$$

where $t_0 < t < t_{\max}$. This family of values is shown in **Figure 8** as black points.

From **Figure 8** it is seen that the initial parameters of the ionosphere lie in a very narrow range. It is approximately 0.6 km in h' and 0.015 km^{-1} in β. The dispersion of the ionospheric parameters at the time of maximum flare is approximately the same in h' and 10 times larger in β (about 0.15). This is due to the fact that the flash was sufficiently powerful and at the time of the maximum X-ray flux, the "rigidity" of the upper wall of the waveguide became so large that its further increase had virtually ceased to influence the amplitude-phase characteristics of the received signals.

Further, for the initial parameters of the ionosphere that we calculated (i.e., h' = 70.7 and β = 0.33 km^{-1}), we can use Eq. (5) to continue the calculation of the parameters of the ionosphere for another time: during the decay phase of the X-ray flux, i.e., for time $t > t_{\max}$, and for the time before flash, i.e., $t < t_0$. Thus, we can restore the time history of the parameters h' and β for the X-ray flash. These results are shown in **Figure 9b**. This figure clearly shows the advantage of our method. It can be seen how the parameters of the ionosphere changed before the flash from 11:30 to 11:55 UT. The parameter h' changed from 69.5 to 71 km and the β parameter from 0.36 to 0.33 km^{-1}. This is due to the relaxation of the ionosphere after the previous flare of class X2.2 that occurred at 9:00 UT. The same method was used for
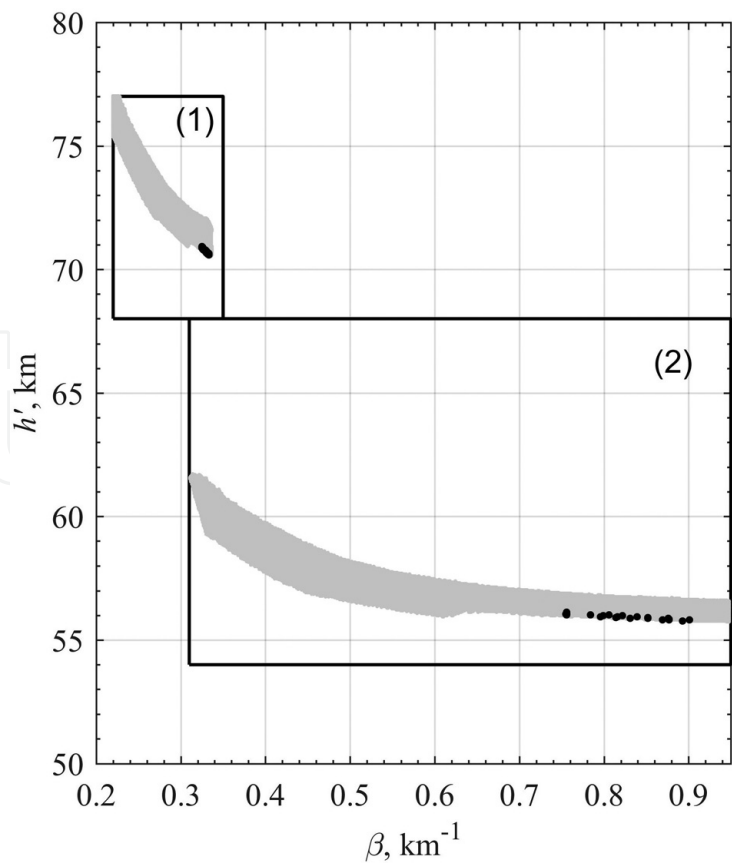
Figure 8.
The regions of ionospheric parameters h' and β before the flash Eq. (1) and at maximum X-ray radiation Eq. (2). The regions of existence of pairs of points (h$_o$', β$_o$) and (h$_{max}$', β$_{max}$) that satisfy the condition Eq. (4) are extended gray areas.
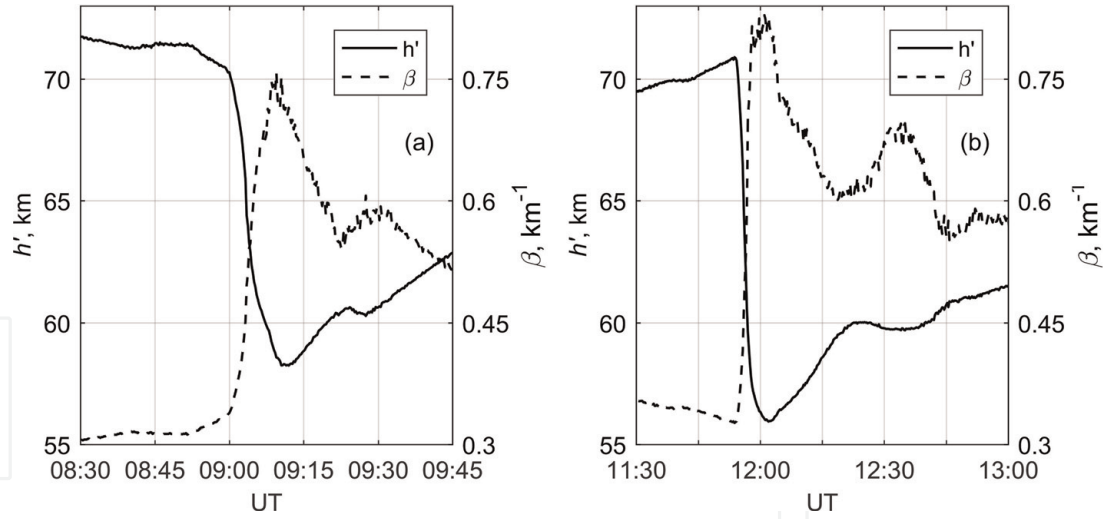
Figure 9.
The time history of the lower ionosphere parameters h' and β for the X2.2 flash (a) and for the X9.3 flash (b) on 6 September 2017.

X2.2 flash at 9:00 UT on 6 September 2017. The results of these calculations are shown in the **Figure 9a**.

Knowing the parameters h' and β of the altitude profile of the electron concentration in the D region, it is possible to calculate the electronic content in it. Let us call this parameter DEC. To do this, the value of the electron concentration, that is, defined by Eq. (2), must be integrated in height in according to

$$DEC = \int_{50}^{h'+\delta h} 1.49 \cdot 10^7 \cdot e^{(\beta-0.15)\left(z-h'\right)} e^{-0.15h'} dz \qquad (6)$$

The lower limit of integration is not very important, since according to Eq. (2) for small z, the electron concentration of N_e is minimal. But there is a problem of choosing the upper limit of integration. This is due to the fact that the according to Eq. (2), the ionosphere shows the exponential growth of the electron concentration with height. At the same time, the electromagnetic wave cannot penetrate into the region of high concentrations and, therefore, does not carry any information about the state of the ionosphere at these heights. So, the VLF radio waves should be reflected in a layer of thickness of the order of wavelength. Therefore, it would be reasonable to carry out the integration up to the height $h' + \delta h$, where δh is a value comparable to the wavelength.

Now consider the effect of solar X-ray flares in the upper and lower ionosphere comparing the change in TEC of the ionosphere according to GNSS receiver data to electronic content in the D region (let us call this parameter DEC), according to the parameters of VLF radio signals.

Figure 10 shows DEC and TEC variations caused by flashes X2.2 (a) and X9.3 (b) on 6 September 2017. Here, to calculate DEC the integration of the electron density N_e was carried out up to a height of $h' + 12$ km. TEC was calculated from the GPS receiver data installed in the Mikhnevo observatory.

You can see that at the solar flash X2.2, (a) the amplitude of the increase in TEC and DEC was about four times less than during the flash X9.3. So, the change of the amplitude of the perturbations of both the upper and lower ionosphere was directly proportional to the change in the X-ray flux. But the most interesting result of these measurements is the proximity of the electron density perturbations in the

upper and lower ionosphere. This result shows that the increase in TEC in both cases was provided by an increase in the electron concentration in the lower ionosphere.

Figure 11 shows the deviations of TEC from the median value over the preceding month of 6 September 2017. This map was constructed from the Madrigal navigation network by using algorithm Eq. (1) as in the previous section. Comparison of **Figures 4** and **11** shows that the maximum deviation of TEC during a solar flare is about four times less than in the main phase of a strong magnetic storm.
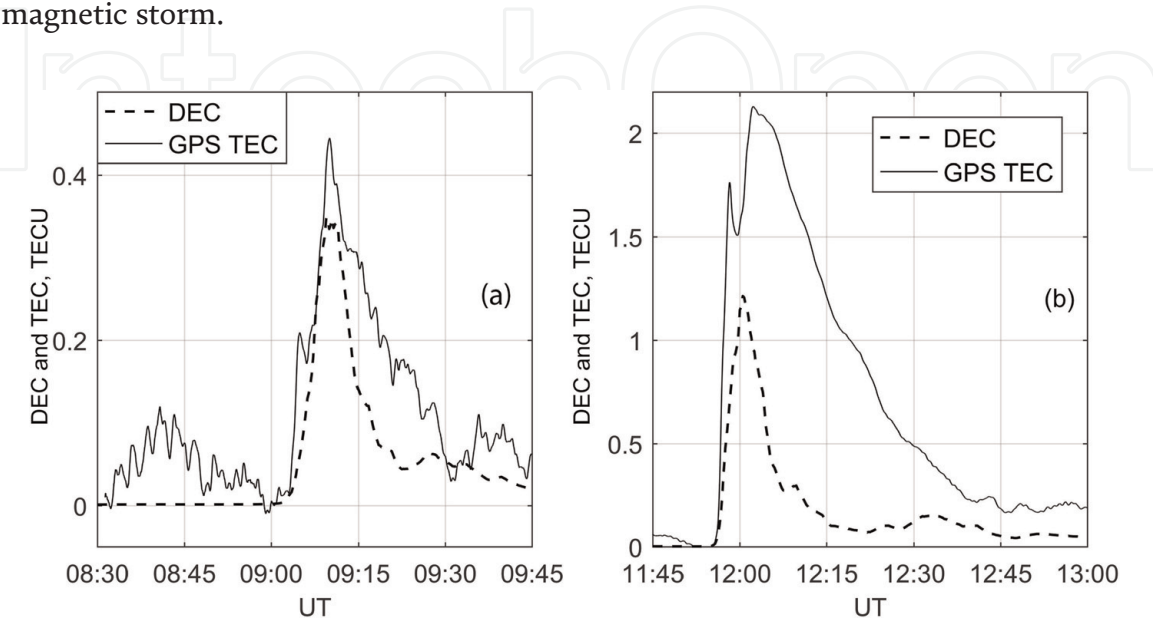
Figure 10.
Variations of DEC and TEC during solar flashes X2.2 (a) and X9.3 (b) on 6 September 2017.
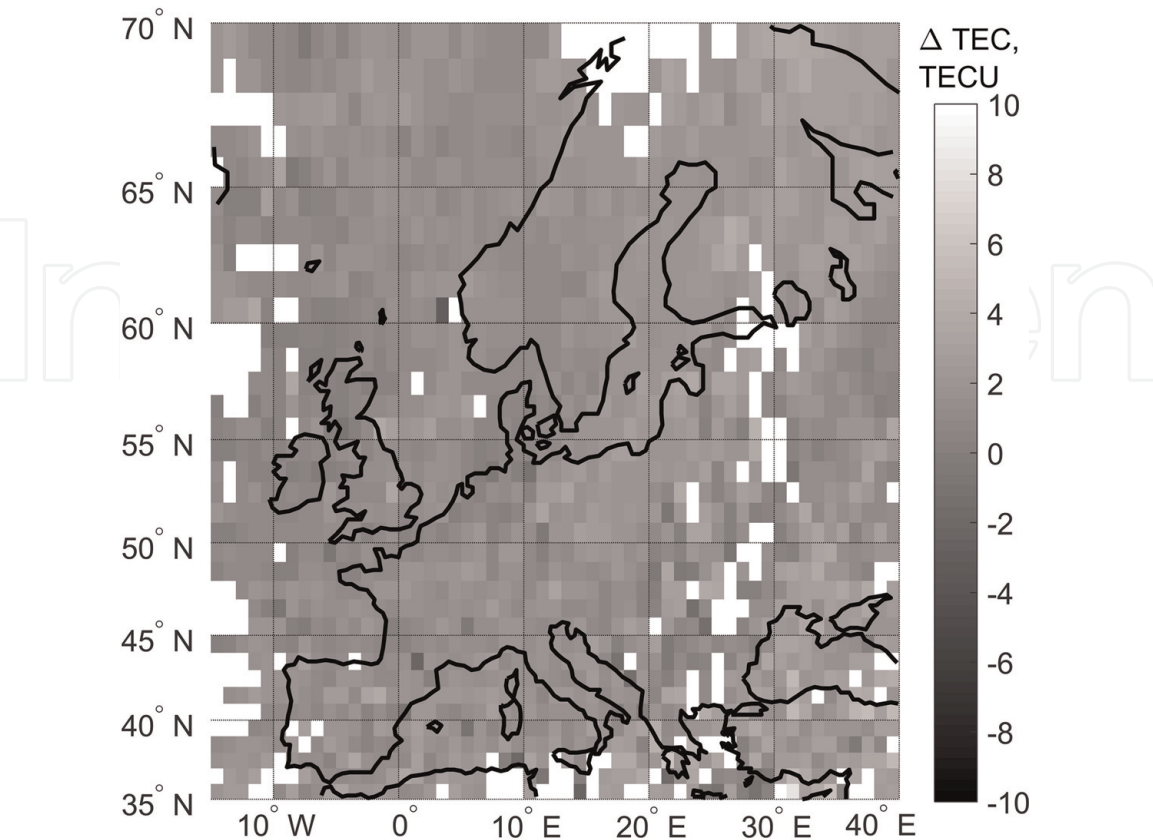
Figure 11.
The ΔTEC value determined by Eq. (1) for 6 September 2017.

5. Conclusion

The study of the influence of heliogeophysical phenomena on the conditions of GNSS functioning was carried out under strong magnetic storms and powerful solar X-ray flares. Experiments on these types of events were carried out in one latitudinal zone using one set of data sources. This allows not only to study the disturbances of the upper and lower ionospheres for different geophysical processes but also to compare their nature and magnitude.

The combined analysis of data from GPS receivers, data from the Madrigal network, and data from measurements of VLF radio signals provides a fairly complete picture of the effects caused by X-ray flashes and magnetic super storm in the upper and lower ionospheres.

Both during the solar X-ray flares on 6 September 2017 and during the magnetic storm on 17 March 2015, the significant changes in the electron concentration of the ionosphere were observed. But the amplitude of these changes and most importantly the ratio of the growth of the electron concentration in the D and F regions of the ionosphere differed significantly in these two events.

During the geomagnetic storm on 17 March 2015, TEC disturbances and VLF signal variations correspond to its main phase. TEC increase was about 15–20 TECU (**Figure 2a**). The perturbation of the F layer at solar X-ray flares was much lower and did not exceed 2.5 TECU (**Figure 5a**), so it was approximately eight times less than during the magnetic storm.

Comparison of TEC estimated from the Madrigal GPS network (**Figures 4** and **10**) with the data obtained for individual stations is not correct. However, it can be seen that according to Madrigal, TEC increase during the magnetic storm was significantly stronger. It is also obvious that during the solar flashes, there is a much more uniform distribution of TEC, as it should be in the conditions of illumination by the radiation of the flash throughout Europe.

The analysis of the results of VLF radio signal amplitude variations on the paths from several European and American VLF transmitters to the receiver at Mikhnevo observatory during St. Patrick's Day magnetic storm on 17 March 2015 and solar X-ray flares on 6 September 2017 shows the effects of the both events to the lower ionosphere as well.

To estimate the lower ionospheric contribution to the TEC value, we have developed a method for restoring the high-altitude profile of electron concentration in the D region of the ionosphere by using the amplitude and phase characteristics of signals from VLF transmitters on a two-frequency path.

This method is based on known approaches to solving this problem [17–19]. But if in these works the determination of the parameters of the lower ionosphere was carried out by analyzing the contribution to the ionization of X-ray radiation and as the initial (before the flash) parameters of the ionosphere were used parameters determined by models, our technique allows to calculate parameters of the lower ionosphere, in which it was before the disturbance using only the measurement data.

A comparison of TEC value calculated from GPS receiver data with the calculation of the electron content in the D region from the data of the VLF radio signal parameters indicates the possibility of a significant contribution of the lower ionosphere, at least during the powerful X-ray flashes.

We have not been able to calculate DEC for magnetic storm conditions. Changing the parameters of VLF signals was complex and ambiguous. However, the fact that the increase in the amplitudes of VLF signals during the storm was close to the growth of this value during solar X-ray flares and the growth of TEC in a storm significantly exceeded the growth of TEC during solar X-ray flares clearly indicates

a substantially smaller contribution of DEC to TEC in a magnetic storm than in solar X-ray flares.

So, the combined analysis of variations of GNSS signals and signals from VLF radio stations is an effective method for studying the interrelated processes in the upper and lower ionosphere [23, 24].

We believe that an important result of our research is to demonstrate that the interpretation of data on the total electronic content of the ionosphere obtained from the data of GNSS receivers should take into account the contribution that can make to the TEC value by the change of electron concentration in the lower ionosphere. On the other hand, the occurrence of significant electron density perturbations in the lower ionosphere should be taken into account in the analysis of factors affecting the accuracy and reliability of GNSS operation.

Acknowledgements

Author details

Boris Gavrilov*, Yuriy Poklad and Iliya Ryakhovskiy
Institute of Geosphere Dynamics RAS, Moscow, Russian Federation

*Address all correspondence to: boris.gavrilov34@gmail.com

IntechOpen

References

[1] Afraimovich EL, Boitman ON, Zhovty EI, et al. Dynamics and anisotropy of traveling ionospheric disturbances as deduced from transionospheric sounding data. Radio Science. 1999;**34**(2):477-487. DOI: 10.1029/1998RS900004

[2] Demyanov VV, Yu V. Yasyukevich S, Jin S. Effects of solar radio emission and ionospheric irregularities on GPS/GLONASS performance. In: Jin S, editor. Geodetic Sciences – Observations, Modeling and Applications. InTech; 2013. pp. 177-222. ISBN: 978-953-51-1144-3. DOI: 10.5772/54568

[3] Demyanov VV, Zhang X, Lu X. Moderate geomagnetic storm condition, WAAS alerts and real GPS positioning quality. Journal of Atmospheric Science Research. 2019;**2**(1). DOI: 10.30564/jasr.v2i1.343

[4] Ryakhovskiy IA et al. Ionization of the lower ionosphere during the X-ray solar flare on September 6, 2017. In: Proceedings of SPIE 10833, 24th International Symposium on Atmospheric and Ocean Optics; 2018. p. 108339Y. DOI: 10.1117/12.2504402

[5] Demyanov VV, Yasyukevich YV. GNSS carrier phase noise as a promising means to reconstruct fine structure of the ionosphere. Journal of Aeronautics & Aerospace Engineering. 2018;**7**:60. DOI: 10.4172/2168-9792-C1-22

[6] Afraimovich EL, Astafyeva EI, Demyanov VV, Gamayunov IF. Mid-latitude amplitude scintillation of GPS signals and GPS performance slips. Advances in Space Research. 2009;**43**: 964-972. DOI: 10.1016/j.asr.2008.09.015

[7] Afraimovich EL, Ding F, Kiryushkin V, Astafyeva E, Jin S, San'kov V. TEC response to the 2008 Wenchuan earthquake in comparison with other strong earthquakes.

International Journal of Remote Sensing. 2010;**31**(13):3601-3613. DOI: 10.1080/01431161003727747

[8] Hayakawa M, Molchanov OA. Seismo Electromagnetics: Lithosphere-Atmosphere-Ionosphere Coupling. Tokyo: Terra Sci.; 2008. p. 477

[9] Perevalova NP, Sankov VA, Astafyeva EI, Zhupityaeva AS. Threshold magnitude for ionospheric TEC response to earthquakes. Journal of Atmospheric and Solar-Terrestrial Physics. 2014;**108**:77-90

[10] Kumar A, Kumar S. Space weather effects on the low latitude D-region ionosphere during solar minimum. Earth, Planets and Space. 2014. p. 76. DOI: 10.1186/1880-5981-66-76

[11] Gavrilov BG, Zetser Yu I, Ryakhovskii IA, Poklad Yu V, Ermak VM. Remote sensing of ELF/VLF radiation induced in experiments on artificial modification of the ionosphere. Geomagnetism and Aeronomy. 2015;**5**(4):450-456. DOI: 10.7868/S00016794015040045

[12] Han F, Cummer SA, Li J, Lu G. Daytime ionospheric D region sharpness derived from VLF radio atmospherics. Journal of Geophysical Research. 2011;**116**(5). DOI: 10.1029/2010JA016299

[13] Maurya AK, Veenadhari B, Singh R, et al. Nighttime D region electron density measurements from ELF-VLF tweek radio atmospherics recorded at low latitudes. Journal of Geophysical Research. 2012;**117**(A11). DOI: 10.1029/202JA017876

[14] Gavrilov BG, Zetser Yu I, Lyakhov AN, Poklad Yu V, Ryakhovskii IA. Spatiotemporal distributions of the electron density in the ionosphere by records of the total electron content and phase of VLF radio

signals. Geomagnetism and Aeronomy. 2017;**57**(4):461-470. DOI: 10.7868/S001679401704006X

[15] Astafyeva E, Zakharenkova IM, Forste M. Ionospheric response to the 2015 St. Patrick's Day storm: A global multi-instrumental overview. Journal of Geophysical Research, Space Physics. 2015;**120**(10):9023-9037. DOI: 10.1002/2015JA021629

[16] Borries C, Mahrous AM, Ellahouny NM, Badeke R. Multiple ionospheric perturbations during the Saint Patrick's Day storm 2015 in the European—African sector. Journal of Geophysical Research, Space Physics. 2016;**121**(11):11333-11345. DOI: 10.1002/2016JA023178

[17] Ferguson J, Snyder FP. Computer programs for assessment of long wavelength radio communications. Tech. Doc. 1773, DTIC AD-B144 839. Alexandria, VA: Naval Ocean System Center, Defense Technical Information Center; 1990

[18] Wait JR, Spies KP. Characteristics of the Earth—Ionosphere waveguide for VLF radio waves. Natl. Bur. of Stand. Technical Note; Boulder, Colo; 1964. p. 300

[19] Basak T. Study of the effects on lower ionosphere due to solar phenomena using very low frequency radio wave propagation [thesis]. Department of Physics, University of Calcutta; 2013

[20] Thomson NR. Experimental daytime VLF ionospheric parameters. Journal of Atmospheric and Terrestrial Physics. 1993;**55**(2):173-184. DOI: 10.1016/0021-9169(93)90122

[21] Davis RM, Berry LA. A revised model of the electron density in the lower ionosphere. Tech. Rept TR I I l-77. Defense Commun. Agency Command Control Tech. Center, Washington, DC. NTIS, AD 17883. 1997. p. 58

[22] Gambill B. Normal D-region models for weapon effects code. Defence Nuclear Agency Report. DNA 62715H; 1985

[23] Gavrilov BG, Zetser YI, Lyakhov AN, Poklad YV, Ryakhovskii IA. Correlated disturbances of the upper and lower ionosphere from synchronous measurements of parameters of GNSS signals and VLF radio signals. Cosmic Research. 2019;**57**(1):36-43. DOI: 10.1134/S0010952519010039

[24] Lyakhov AN, Korsunskaya JA, Poklad YV, et al. The numerical simulation of the 2017 september solar X-flares impact on the midlatitude lower ionosphere. In: Proceedings of SPIE 10833, 24th International Symposium on Atmospheric and Ocean Optics; 108339M; 2018. DOI: 10.1117/12.2504292